



A pipeline for the generation of synthetic cardiac color Doppler

Yunyun Sun, Florian Vixege, Faraz Khuram, Simon Mendez, Franck Nicoud,
Damien Garcia, Olivier Bernard

► To cite this version:

Yunyun Sun, Florian Vixege, Faraz Khuram, Simon Mendez, Franck Nicoud, et al.. A pipeline for the generation of synthetic cardiac color Doppler. IEEE Transactions on Ultrasonics, Ferroelectrics and Frequency Control, 2022, 69 (3), pp.932-941. 10.1109/TUFFC.2021.3136620 . hal-03538666

HAL Id: hal-03538666

<https://cnrs.hal.science/hal-03538666>

Submitted on 13 May 2022

HAL is a multi-disciplinary open access archive for the deposit and dissemination of scientific research documents, whether they are published or not. The documents may come from teaching and research institutions in France or abroad, or from public or private research centers.

L'archive ouverte pluridisciplinaire **HAL**, est destinée au dépôt et à la diffusion de documents scientifiques de niveau recherche, publiés ou non, émanant des établissements d'enseignement et de recherche français ou étrangers, des laboratoires publics ou privés.

A pipeline for the generation of synthetic cardiac color Doppler

Yunyun Sun, Florian Vixège, Khuram Faraz, Simon Mendez, Franck Nicoud, Damien Garcia, and Olivier Bernard

Abstract—Color Doppler imaging is the modality of choice for simultaneous visualization of myocardium and intracavitary flow over a wide scan area. This visualization modality is subject to several sources of error, the main ones being aliasing and clutter. Mitigation of these artifacts is a major concern for better analysis of intracardiac flow. One option to address these issues is through simulations. In this paper, we present a numerical framework for generating clinical-like color Doppler imaging. Synthetic blood vector fields were obtained from a patient-specific computational fluid dynamics CFD model. Realistic texture and clutter artifacts were simulated from real clinical ultrasound cine-loops. We simulated several scenarios highlighting the effects of *i)* flow acceleration, *ii)* wall clutter, and *iii)* transmit wavefronts, on Doppler velocities. As a comparison, an “ideal” color Doppler was also simulated, without these harmful effects. This synthetic dataset is made publicly available and can be used to evaluate the quality of Doppler estimation techniques. Besides, this approach can be seen as a first step towards the generation of comprehensive datasets for training neural networks to improve the quality of Doppler imaging.

Index Terms—Simulations Ultrasound simulator, Color Doppler, Flow imaging, Echocardiography.

I. INTRODUCTION

Doppler echocardiography is the clinical imaging modality of choice for flow analysis in the cardiac chambers. Several Doppler techniques can be used to assess velocities in ultrasound imaging: *i)* Continuous-wave Doppler (CWD) to estimate a wide range of velocities along a predefined ultrasound line; *ii)* Pulsed-wave Doppler (PWD) to estimate velocities within a small spatial volume; *iii)* Color Doppler imaging (CDI) to estimate velocities over a large scan area. Regardless of the mode used, Doppler velocities represent projections of the actual velocity vectors along the ultrasound lines, thus providing incomplete one-dimensional information of the blood velocity field. Spectral Doppler (CWD and PWD) is used to locally estimate blood velocity in specific situations, such as in the assessment of aortic stenosis severity [1]. The ultrasound wave must be carefully aligned with the flow to obtain Doppler velocities closely related to the actual blood speeds. In contrast, CDI is generally used as a visualization modality to display simultaneously the myocardium and intracavitary flow, although at a relatively low frame rate.

CDI is subject to several sources of errors, the main ones being aliasing and clutter noise. Aliasing occurs whenever the velocities to be measured exceed the Nyquist limit, whose value depends on the pulse repetition frequency (PRF) and the pulse center frequency [2]. In the classic red-blue Doppler

color map, when aliased, color-encoded velocities wrap around such that color information turns from red to blue or vice versa [3]. Clutter corresponds to different sources of noise that mainly affect the low-frequency content of the slow-time signals. In echocardiography, clutter is mostly due to the motion of highly reflective tissues that surround the blood cavity. Therefore, blood signals must be separated from clutter before flow estimation.

Several approaches have been proposed to remove aliasing [4], [5] and reduce clutter noise [6], [7]. These techniques are mostly based on standard signal and image processing, which may lead to inherent difficulties in ambiguous and non trivial situations [8]. A recent study reports a deep learning (DL) solution to address the problem of aliasing removal [8]. The proposed method involved a conventional U-Net architecture [9] to localize aliased and double-aliased regions based on information derived from I/Q signals (*i.e.* Doppler frequency, power, and bandwidth, speckle flow angle, and speckle flow speed). Once detected, the aliased regions were corrected using a phase unwrapping algorithm as in [5]. Since the input of the U-Net method uses physical information, it was necessary to apply a clutter filter at the beginning of the workflow. These results illustrate the capability of DL to segment regions with single or double aliasing. Combined with classical signal processing tools, this DL approach demonstrated its ability to improve the quality of flow visualization by CDI.

DL methods have revolutionized several fields of application in ultrasound imaging, the main ones being related to classification (*e.g.* automatic view recognition [10]) and segmentation (*e.g.* automatic extraction of clinical indices [11]). In light of these successes, one may wonder why no additional work has been done so far to improve CDI. One of the main reasons is probably the difficulty of accessing referenced datasets, *i.e.* data whose flows are known and which can be used as a reference for learning algorithms. In this context, ultrasound simulations can play a key role in building such datasets. In this regard, our recent pilot study has shown that DL techniques can learn from synthetic ultrasound sequences to improve a targeted task; in this case, the estimation of rotational movements on *in vitro* data [12].

Computational ultrasound imaging has been applied for the analysis of the myocardial motion from B-mode sequences [13], [14], [15], [16], [17]. Most of the studies involved an electromechanical model (E/M) to generate ground-truth myocardial deformation fields. The E/M model has the advantage of relating cardiac contraction to its biophysical causes, allowing the inclusion of physiological and pathological conditions [18]. Prakosa *et al.* first proposed a warping-based method where a real B-mode sequence was registered to the E/M simulations [13]. Although the resulting images

Y. Sun, K. Faraz, F. Vixège, D. Garcia and O. Bernard are with CREATIS, CNRS UMR 5220, INSERM U1294, INSA-Lyon, University of Lyon 1, Villeurbanne, France. E-mail: olivier.bernard@creatis.insa-lyon.fr. S. Mendez and F. Nicoud are with the IMAG, Univ Montpellier, CNRS, Montpellier, France.

showed realistic textures, warping defects degraded the quality of the synthetic images. To reduce those warping artifacts, De Craene *et al.* [14] used the ultrasound simulator FieldII to generate ultrasound images. However, the scatterers were too simplistic, yielding unrealistic binary-like synthetic ultrasound images. To solve this issue, Alessandrini *et al.* combined the E/M model, an ultrasound simulator, and B-mode template images into a unified pipeline [19]. Their simulation pipeline combined the advantages of both [13] and [19], and was able to produce realistic synthetic images. However, the backscattering transition between the myocardium and the surrounding environment was not sufficiently controlled, reducing the degree of realism of the simulated sequences. To solve this issue, the authors of two recent studies ([16] and [20]) introduced different strategies to ensure a smoother transition between the myocardium and the blood pool, leading to realistic B-mode echocardiographic imaging simulations (both 2D and 3D). The use of the electromechanical E/M model remains, however, the Achilles heel if a wide spectrum of simulations is required.

A. Main contributions

In comparison with the literature, the main novelties introduced in this paper are:

- the development of a simulation pipeline for the generation of clinical-like duplex ultrasound sequences, *i.e.* the simulation of both B-mode and Doppler images.
- the inclusion of a patient-specific computational fluid dynamics (CFD) model into our simulations to produce ground-truth blood vector fields.
- the introduction of controlled clutter noise through simple modeling of myocardial motion.
- the assessment of the validity of our pipeline by simulating different synthetic duplex sequences.

II. METHODOLOGY

Fig. 1 provides the flowchart of the color Doppler simulation pipeline. In the following, we call “template” any real (clinical) duplex acquisition. The next sections (Sec. II-A, Sec. II-B, Sec. II-C) describe the content of each block. Clinical apical long-axis 3-chamber B-mode recordings are used to simulate sequences with realistic tissue texture. The first step of the simulation pipeline is to delineate the endocardium on the template cine-loop. Two regions of interest (ROIs) are then obtained: the intraventricular cavity, and the left ventricular myocardium. Time-varying surface meshes are generated for both ROIs (block A in Fig. 1). Using these echo-derived meshes, a CFD intracardiac flow is anchored to the intracavity ROI of the template cine-loop by spatio-temporal registration. It provides a ground-truth sequence of intracardiac blood motion (block B). This reference motion is then used to displace blood point-scatterers, inside the left ventricle, from one simulated frame to the next (block C). As for the myocardial meshes, they are used to move the myocardial scatterers to produce realistic B-mode images and clutter in the Doppler signals. An ultrasound open-source simulator (SIMUS) is finally run on the blood + myocardium scatterer maps to generate synthetic

ultrasound signals. These signals are post-processed with conventional beamforming and Doppler algorithms to construct duplex ultrasound cine-loops.

A. Pre-processing

1) *Template image sequences*: A clinical 2-D ultrasound acquisition was used as a template sequence to set the geometry and provide the texture of the simulated ultrasound images. The 2-D sequences (one complete cardiac cycle between two end-diastoles ED1 and ED2) were acquired from an apical three-chamber view using a GE Vivid e9 ultrasound scanner (GE Healthcare) and a 2.5 MHz phased array. All sequences were acquired in duplex mode to obtain both B-mode and Doppler images during a routine clinical examination. The ultrasound machine settings were adjusted to scan the entire left ventricular cavity and myocardium, from the apex to the base. It returned a pulse repetition frequency (PRF) of ~ 7000 , and a frame rate of 16 fps. All the subjects were scanned with nearly identical conditions.

2) *Manual segmentation*: The template sequences were segmented manually to get contours over the cardiac cycle. We defined eight instants evenly spaced between ED1 and ED2. Endocardial and epicardial borders were delineated manually at each instant. Each boundary was then resampled to ensure an even distribution of points along the contours. These points were finally interpolated in time using periodic spline to obtain myocardial and intracavity ROIs over the entire cardiac cycle. Once the endocardial and epicardial contours have been manually segmented, the myocardial and left ventricular meshing procedures are fully automatic.

3) *Myocardial meshes*: The left side of Fig. 2 illustrates the myocardial meshing. For each myocardial ROI, the base of the left ventricle was defined by the line linking point #1 (pt1) to point #2 (pt2). We defined the apex as the point of the epicardial contour whose distance from the base was greatest. 36 points were then evenly distributed over the epicardial contour: 18 on the lateral wall, and 18 on the anterior wall. Intramyocardial segments perpendicular to the epicardial contour and passing through the 36 epicardial points were then automatically drawn to join the epicardial and endocardial contours. Each intramyocardial segment contained 5 evenly distributed points. This resampling scheme allowed myocardial meshing with 180 points ($36 \text{ longitudinal} \times 5 \text{ radial}$) and 280 triangle cells. These myocardial meshes were used in Sec. II-C to compute the myocardial displacements.

4) *Left ventricle meshes*: The right side of Fig. 2 illustrates the left ventricular intracavitary meshing. As with the myocardial meshes, the basal and apical points were computed automatically from the intracavity ROIs. 21 points were evenly distributed over the endocardial contour. The basal and apical points were used to define the median axis of the left ventricular ROI cavity (see Fig. 2, right panel, gray curve). Two-thirds of the median axis were sampled uniformly, and the corresponding points (green points along the median axis) were associated with their endocardial counterpart to define linear 4-point segments. The apical region was sampled spherically.

This resampling scheme allowed intracavitary meshing with 71 points (15 apical + 56 basal) and 114 triangle cells. These left ventricular intracavitary meshes were used in Sec. II-B to register a ground-truth blood flow motion on the template sequences.

B. Blood flow motion

1) *CFD model*: To incorporate a reference blood-motion field into our simulations, we used a patient-specific heart flow CFD model developed by Chnafa *et al.* [21]. In this CFD model, the cardiac cavities and the wall dynamics were extracted from 4-D clinical images acquired by computed tomography. The CFD computation was based on an ALE (Arbitrary Lagrangian-Eulerian) method. The ALE method is a way to couple Eulerian and Lagrangian formulations to solve fluid-structure coupling problems. This CFD model provided complex 3-D flow motion in a complete left heart including the left ventricle, the left atrium, and the aorta inlet. More details on the CFD model can be found in [21], [22], [23]. From this model, an apical three-chamber view was reproduced by locating the probe at the apex, with the sector enclosing the mitral inlet and the left ventricular outflow tract (left part in Fig. 3), as in [24]. In this study, we limited ourselves to planar simulations. Out-of-plane blood motions (in the elevation direction) of the insonified scan-area were not considered since the ultrasound simulations were two-dimensional (see Sec. II-D).

2) *Spatio-temporal registration*: Fig. 3 illustrates the spatio-temporal registration we computed to anchor the CFD intracardiac flow to the template cine-loop. We first used a piece-wise linear transformation to match the end-diastole and end-systole times of the CFD model with those of the template sequence. The orange dots in Fig. 3 were used as temporal landmarks to perform this temporal registration. Time-varying surface meshes for the intraventricular cavity of the CFD model were then generated using the same procedure as that described in Sec. II-A4. Each point of the CFD meshes was finally registered to the corresponding template meshes by interpolating the position of the corresponding cell. This procedure was used to spatio-temporally register one blood flow map per emitted beam on the template cine-loop. It modified both the amplitudes and directions of the velocity vectors. The mechanical properties of the flow were therefore not totally conserved. For example, the conservation of mass was affected. Our goal here was to obtain clinical-like Doppler images from an imaging point of view, not from a mechanical point of view.

C. Myocardial motion

Our simulation pipeline includes the motion of the myocardium to generate synthetic clutter in left ventricular color Doppler. The myocardial motion was not simulated with the electromechanical model that we used in [20]. For each simulation, a set of points was randomly distributed over the myocardial mesh at end-diastole. Each of these points was then propagated over the full sequence by interpolating the

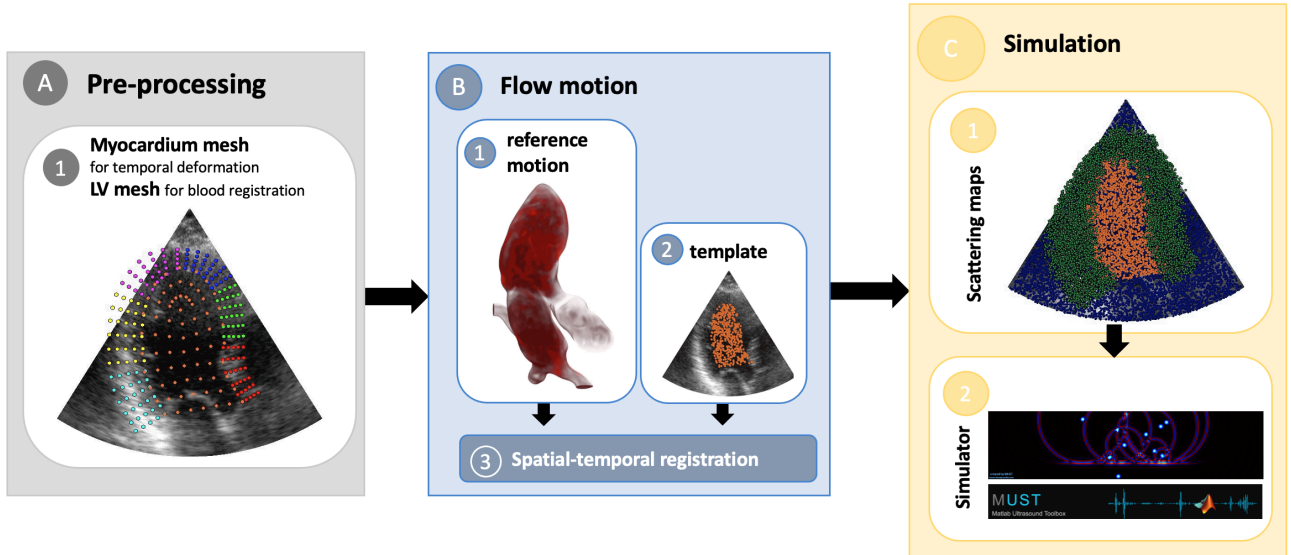


Fig. 1: Proposed pipeline for the simulation of clinical-like duplex ultrasound sequences. (A) A clinical recording works as a template for speckle texture, anatomy definition, and myocardial motion estimation; (B) A CFD model controls the synthetic blood flow motion; (C) An ultrasound simulation environment merging information from the template image sequence and the CFD model accounts for the image formation process. In the simulated sequence, the blood flow is fully controlled by the CFD model while the visual appearance is very similar to the one of a real acquisition. Each block specifies the section number where the description is detailed.

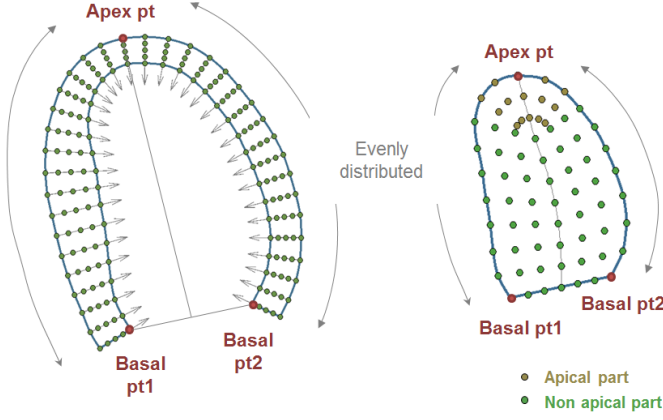


Fig. 2: Meshing of the segmentation masks for the myocardium (left) and left ventricular cavity (right). The proposed schemes allowed myocardial meshing with 180 points (36 longitudinal \times 5 radial) and 280 triangle cells, and intracavitary meshing with 71 points (15 apical + 56 basal) and 114 triangle cells.

displacements of the corresponding cell. This simple procedure allowed us to compute applicable temporal trajectories of any point belonging to the myocardium.

D. Ultrasound duplex simulation

Our pipeline uses a homemade open-source software called SIMUS from the MUST Matlab ultrasound toolbox (<https://www.biomecardio.com/MUST>) [25]. SIMUS simulates backscattered ultrasonic signals for linear, phased, and convex arrays [26]. It allows the simulation of ultrasound images from different transmission schemes (*i.e.* using focused beams, plane waves or diverging waves) by adjusting the transmit delay laws. The latest version of the simulator now integrates 3-D acoustics, which was not the case at the time of this study. Our ultrasound simulations were thus planar. The insonified medium is modeled by monopole point sources that do not interact with each other (weak scattering). From the position and reflection coefficient of each scatterer, SIMUS computes the ultrasound signals that are received back by the probe, as illustrated in block C of Fig.1. We used SIMUS to compute the B-mode and Doppler cardiac images (duplex sequences). The same probe settings used to acquire the real B-mode sequence were simulated: a 2.5 MHz 64-element cardiac phased array emitted at a PRF of 7000 Hz. The bandwidths at -6dB were respectively 60% and 20% for the B-mode and Doppler sequences, which corresponded to transmit pulses of 2 and 6 wavelengths. Assuming a heart rate of 60 beats per minute, a focused-beam configuration returned sixteen 11-cm deep B-mode frames interleaved with color Doppler images obtained with packet lengths of 8.

1) *Realistic B-mode sequence*: The overall strategy for the simulation of the B-mode sequence is illustrated in Fig. 4. Each B-mode frame was generated by transmitting 90 focused beams.

Background scatterer maps: N_{back} scatterers were randomly

distributed in the sector of the first template image. The scatterer density was 10 per square wavelength, which corresponded to $N_{back} \approx 250,000$. To avoid flickering effects, the background scatterers were kept motionless. We set the reflection coefficients of the scatterers to generate realistic images. To mimic the tissue echogenicity of the recorded model, the local intensities I_m of the actual B-mode images were used to calculate the reflection coefficients RC_m of the scatterers, according to the following expression:

$$RC_m = (I_m/255)^{(1/\gamma)} \cdot \mathcal{N}(0, 1) \quad (1)$$

where $\mathcal{N}(\cdot)$ is the normal distribution, and γ is a constant for gamma compression (set to 0.3).

Myocardial scatterer maps: The scatterers of the myocardium were selected on the first simulated frame. The positions of these scatterers were then computed for each B-mode frame of the simulated sequence using the strategy described in Sec. II-C. The reflection coefficients of these scatterers were kept constant to maintain the speckle texture throughout the cardiac cycle.

Blood scatterer maps: To simulate Doppler information, blood scatterers were added in each B-mode frame of the simulated sequence. These scatterers were randomly distributed in the intracavity ROIs with a density of 10 scatterers per square wavelength and reflection coefficient values following a Gaussian distribution. To mimic the large difference in amplitude between blood and the surrounding tissues, we set a ratio of 70 dB between the RC values of the myocardial and blood scatterers RC_m^{blood} . The following expression was used:

$$RC_m^{blood} = \frac{1}{10^{(70/20)}} \cdot \mathcal{N}(0, 1) \quad (2)$$

Final scatterer maps: The final scatterer maps were obtained by combining the background, myocardial, and blood scatterer maps. The background and myocardial scatterers were combined to ensure a smooth transition at the myocardial borders using the same scheme as described in [20].

2) *Simulation of the Doppler information*: Fig 5 illustrates the scheme we implemented to simulate Doppler images. Blood scatterers were moved between each emitted beam by interpolating their displacements through the template flow maps described in Sec. II-B. Each color Doppler image was generated using 44 focused beams in transmission with packet lengths of 8.

3) *Reconstructed synthetic B-mode and Doppler data*: The synthetic RF signals generated by SIMUS were demodulated to obtain in-phase/quadrature I/Q signals. The I/Q signals were beamformed using a delay-and-sum to obtain B-mode and color Doppler images [27]. For clutter filtering, we removed the mean of the I/Q signals (= zero-order polynomial-regression filter). The Doppler velocities were deduced by using a lag-1 autocorrelator [28].

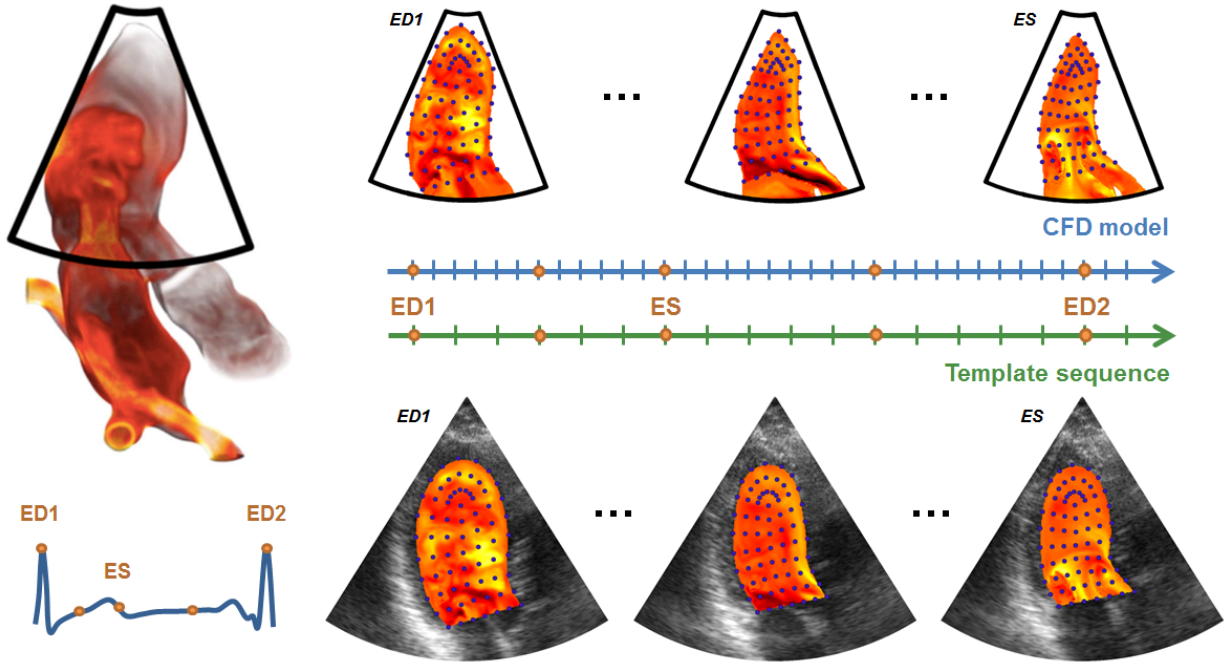


Fig. 3: Illustration of the spatio-temporal alignment used to register the flow of the CFD model to the template sequence. The color map indicates the amplitude of the velocity along the cross-beam x -direction. The orange markers were used as key instants to perform a piece-wise linear registration between the CFD model and the template sequence. Each point of the CFD meshes was registered to the corresponding template meshes by interpolating the position of the corresponding cell.

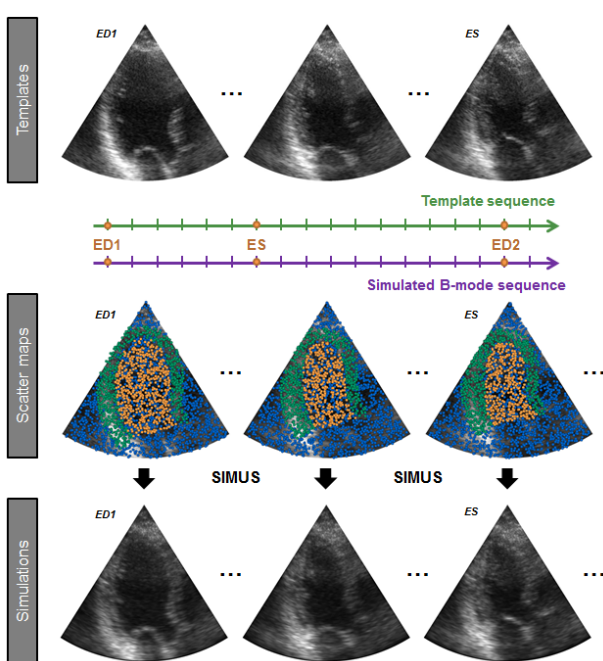


Fig. 4: Overall strategy for the simulation of B-mode sequences. Each B-mode frame of the template sequence was used to define a set of scatterers characterized by their positions and reflection coefficients. This information was then provided into the SIMUS ultrasound simulator to generate synthetic images.

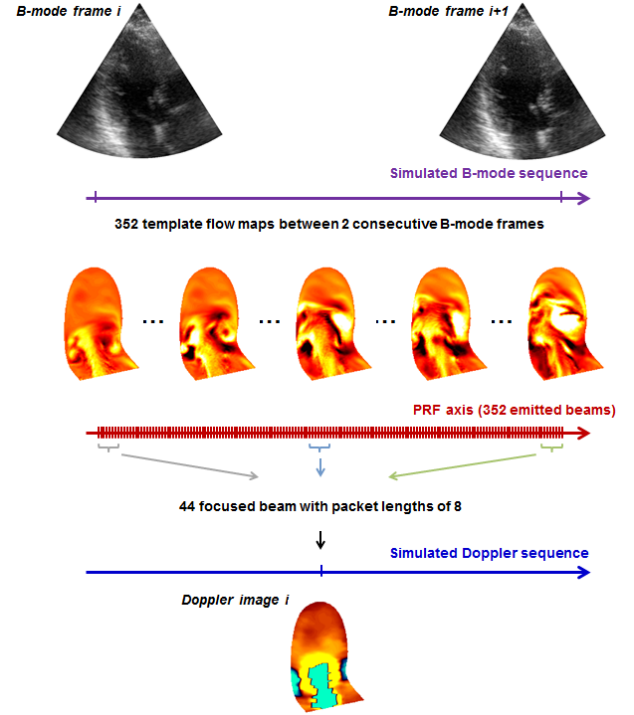


Fig. 5: Overall strategy for the simulation of Doppler images. 352 registered flow maps were used between each consecutive B-mode frame. This leads to a different map per emitted beam at the PRF frequency. 44 focused beams with a packet length of 8 were used to estimate each color Doppler image.

E. Simulated scenarios

Our color Doppler simulation pipeline is flexible enough to generate different types of scenarios. This is interesting in the perspective of generating datasets to feed into DL algorithms to improve the quality of flow visualization and quantification by CDI. To illustrate the relevance of each element of the pipeline, we simulated four scenarios ranging from simplified to more realistic situations for five virtual patients. For each simulation, the generated synthetic sequence and the reference motion field are made available to the community, yielding to an open access dataset composed of 20 benchmarked sequences. This synthetic dataset is accessible at the following link: <http://humanheart-project.creatis.insa-lyon.fr/duplex.html>. The simulation of a full sequence composed by 16 B-mode and color Doppler images took around 4 hours using a C version of the SIMUS code running on an Intel 2 Xeon E5@2.9Ghz with 512GB RAM.

1) *Scenario #1: color Doppler "snapshot"*: This scenario assumes that one would be able to obtain an instantaneous color Doppler image (color Doppler "snapshot") 1) in the absence of myocardial motion, and 2) assuming that the flow is stationary (no temporal acceleration) during the ultrasound emissions generated to obtain this image. The number of emissions to simulate a Doppler image was 352 (44 focused beams with a packet length of 8, as illustrated in Fig. 5). This prevented *i*) the introduction of clutter noise due to the movement of high-intensity tissues and *ii*) the presence of bias during Doppler estimation caused by blood acceleration. In this snapshot scenario, the estimated Doppler velocities should match the radial velocity components of the CFD-based reference flow.

2) *Scenario #2: Doppler simulation of a non-steady-state flow*: Blood motion is no longer quasi-stationary: the blood scatterers are relocated between two successive ultrasound transmits. This scenario takes flow acceleration into account, which has side effects on Doppler estimation. The motion of the blood scatterers was computed using the template flow maps described in Sec. II-D2.

3) *Scenario #3: additional synthetic clutter noise*: In contrast with the other scenarios, the third scenario aims at simulating color Doppler as obtained in a clinical setting. All the blood and tissue scatterers are relocated between two successive ultrasound transmits. In this context, the information carried by the slow motion of the tissues is mixed with that of the blood flow, which led to wall clutter noise.

4) *Scenario #4: focused vs. diverging waves in transmission*: Each color Doppler image presented in the previous scenarios was generated using 44 focused beams in transmission with packet lengths of 8. This led to an accurate estimate but at the cost of a small temporal frequency (*e.g.* 16 fps for the simulated sequences). To work at higher imaging rates, recent works proposed to estimate Doppler velocities from diverging waves [29], [30]. In these conditions, the whole Doppler sector is insonified with each emitted beam, which drastically increases the frame rate of color flow imaging. However, since this strategy spreads the acoustic energy into a large area,

the quality of the Doppler estimate is degraded, especially in situations where high-intensity tissue motion is important. In this context, the goal of this scenario was to investigate the influence of the transmission modes on the quality of estimated velocities. Each sequence was simulated in the "snapshot" conditions with the emission of either focused or diverging beams for the estimation of Doppler information.

III. RESULTS

A. Scenario #1: color Doppler "snapshot"

The second line of Fig. 6 shows Doppler images simulated in the snapshot scenario for different instants during filling, when blood velocity was the highest. From these results, one can appreciate the reliability of the simulated sequence compared to the corresponding Doppler reference given by the radial velocities. Most of the reference flow patterns were simulated and estimated accurately. The small differences are in large part explained by smoothing effects introduced by the Doppler estimator. The simulated color Doppler images also contained aliasing artifacts when the velocities to be measured exceeded the Nyquist limit (1.1 m/s in our case).

B. Towards more realistic scenarios

1) *Scenario #2: Doppler simulation of an unsteady flow*: The third line of Fig. 6 shows images simulated in such conditions for the same instants as those of the snapshot scenario. The Doppler outputs were slightly different since this scenario does not assume stationary flows. The effect of flow acceleration is more visible during the filling phase.

2) *Scenario #3: additional synthetic clutter noise*: Because the information conveyed by the motion of the tissues was mixed with that of the blood flow in this scenario, it was necessary to apply a clutter filter on the synthetic I/Q signals (after beamforming) to recover the blood signals. This was realized using a zero-order polynomial-regression filter. The forth line of Fig. 6 shows images simulated in such conditions. The Doppler outputs were significantly different since this scenario did not provide clutter-free instantaneous maps. The effect of the surrounding myocardial motion during the filling phase is well visible during filling onset. As tissue velocities decreased during the diastolic phase, clutter noise (along the ventricular wall) reduced until it vanished at the end of filling. This is in line with real observations, which illustrates the realism of the simulation pipeline. In addition, Fig. 7 shows the Doppler estimates during the systolic phase in the snapshot scenario compared with the wall-clutter scenario. These results further illustrate the impact of tissue motion on Doppler estimation. In this example, Doppler bias appeared along the blood/tissue interface, especially near the septum where tissue motion was most pronounced.

C. Scenario #4: focused vs. diverging waves in transmission

Fig. 8 displays the results obtained for two instants where the motion of high-intensity tissues was either high (*i.e.* beginning of diastole) or low (*i.e.* diastasis). These results show that the quality of Doppler estimation is related to the amount of

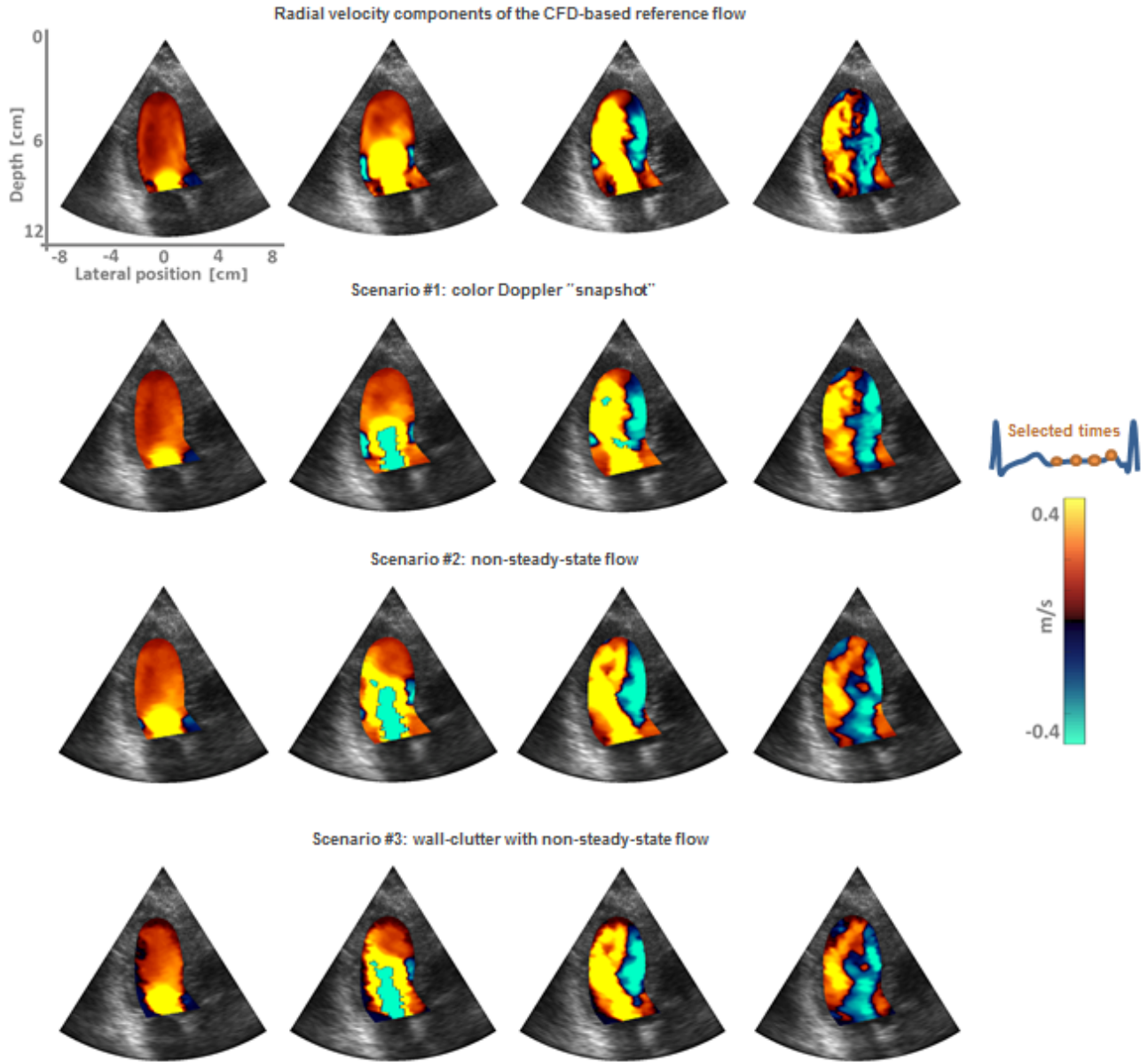


Fig. 6: Illustration of the ability of our Doppler simulation pipeline to generate three different types of scenarios: 1) a color Doppler “snapshot” situation assuming a stationary flow and the absence of myocardial motion (second row); 2) unsteady flow where the blood scatterers are relocated between two successive ultrasound transmits (third row); 3) wall-clutter with unsteady flow where both the blood and tissue scatterers are relocated between two successive ultrasound transmits (fourth row).

tissue motion when diverging waves are used in transmission. Indeed, the clutter phenomenon is more prominent when the motion of high-intensity tissues is important.

D. Evaluation of a Doppler estimation algorithm

Our simulation pipeline can also be used to provide benchmark datasets to assess the quality of Doppler estimation methods. We evaluated the effect of wall filtering in the presence of myocardium-based clutter by using two different datasets: one generated from scenario #1, and another from the same scenario but with additional wall clutter. Each dataset was composed by 16 Doppler images for 5 virtual patients. In each case, the estimated Doppler velocities were compared with the

radial velocity components of the CFD-based reference flow. Fig. 9 displays the mean correlation plots computed over the five virtual patients. Results show a high agreement between the CFD-based and simulated-derived Doppler velocities for the dataset generated from scenario #1, with a coefficient of determination of 0.92. The small differences can be explained by the smoothing effect of the estimator. The degradation induced by the wall clutter noise can be investigated from the right part of Fig. 9. In particular, a decrease of 19% of the coefficient of determination can be observed.

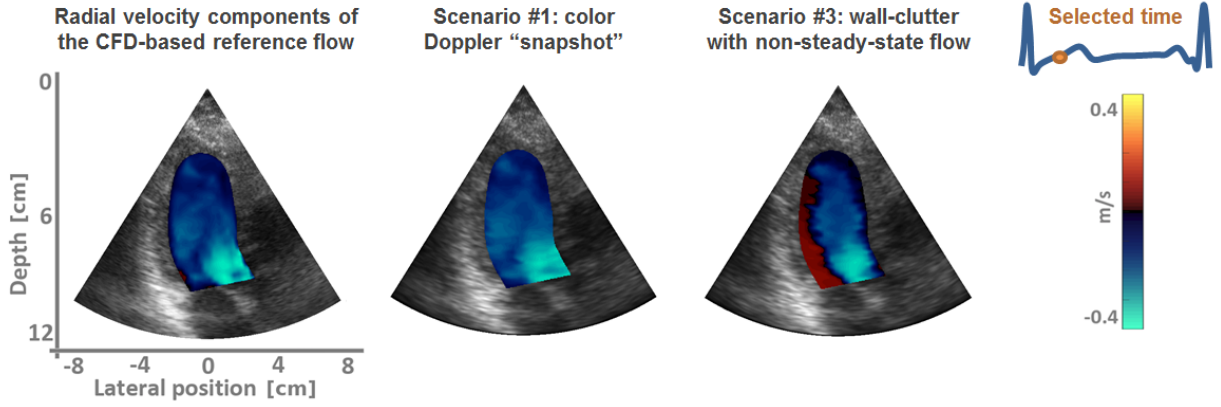


Fig. 7: Color Doppler snapshot vs. wall-clutter scenarios simulated during systolic phase. Large tissue motions along the septum generate synthetic clutter that degrades the color Doppler image estimated from the synthetic I/Q signals.

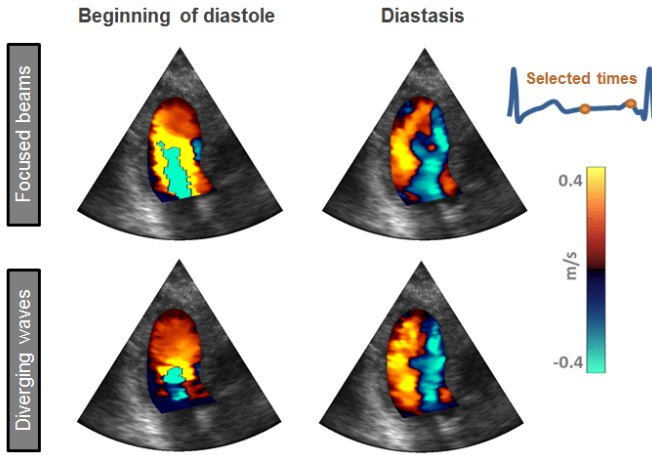


Fig. 8: Focused vs. diverging beams for the estimation of Doppler velocities. While the diverging wave strategy increases the temporal frequency, the spread of the acoustic energy into a large area degrades the quality of the Doppler estimate, especially in situations where the displacements of high-intensity tissues are significantly large.

IV. DISCUSSIONS

A. On the benefits of training DL methods through simulations

Deep learning techniques have been successfully applied to echocardiography for several years. These methods have allowed major advances in many specific areas such as view classification and segmentation of anatomical structures. Almost all the best performing techniques correspond to supervised approaches, requiring the deployment of large-scale datasets with manual annotations. As far as ultrasound motion estimation is concerned, very few referenced data are available, the main one being an open access dataset proposed for myocardial strain benchmarking [20]. A supervised DL network was recently trained on this open-access dataset to automatically estimate myocardial strains [31]. Although the results were very promising, the lack in quantity and diversity of training data did not allow the authors to obtain significantly better scores than the state-of-the-art. Regarding blood

flow estimation, there is currently no baseline dataset. Thus creating large-scale synthetic datasets that mimic hundreds or thousands of patients would be the key to train data-driven DL methods for flow estimation. In this context, we proposed the first simulation pipeline that generates clinical-like duplex ultrasound sequences. Although the size of the derived dataset is not sufficient to train DL models, our framework constitutes the first step toward achieving more complete datasets. A major weakness of our protocol is the need to manually segment the left ventricle and the myocardium throughout the sequence. In the near future, we plan to make this step fully automatic to enhance the scalability of our simulation pipeline, with the goal of creating simulated data that replicates a large number of patients.

B. An innovative simulation pipeline for duplex sequences

The objective of our study was to simulate clinical-like B-mode and color Doppler ultrasound images. By "clinical-like" we mean that these images should resemble those obtained by a cardiologist with a clinical ultrasound machine. For the B-mode images, a set of focused waves scanned the cardiac region, and then a standard delay-and-sum technique was used for image construction. Although the transmission/beamforming scheme may differ from those used by clinical ultrasound scanners, the similarity to clinical images is apparent, particularly with respect to speckle patterns. The realism is also found in the color Doppler simulations. Not only is the similarity observed on the Doppler fields, but also on classical artifact phenomena, such as aliasing and wall clutter.

In this study, we focused only on the generation of clutter due to myocardial motion. We neglected other sources of clutter such as those related to rib reverberations, multi-echoes, or twinkling artifacts [32]. Our goal was not to perform a thorough evaluation but rather to show that our pipeline could generate datasets for the evaluation of Doppler estimation techniques. A thorough investigation is beyond the scope of this paper. The evaluation showed that the datasets can lead to accurate estimates of Doppler velocities in the absence of wall-based clutter. In addition, we quantified the

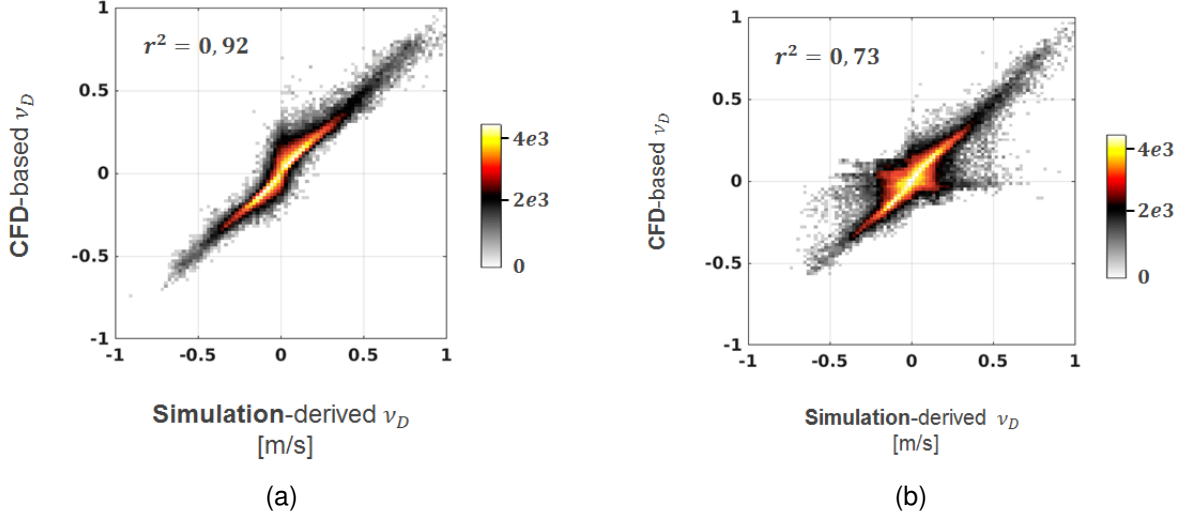


Fig. 9: CFD-based vs, simulation-derived Doppler velocities (v_D) for (a) the scenario #1 and (b) the scenario #1 with additional wall clutter noise. Velocity data from sixteen Doppler images for five different virtual patients.

decrease in color-Doppler performance when wall clutter was present. This is a direct consequence of the motion of highly reflective tissues that surround the blood cavity. This shows the difficulty in developing techniques that are robust to the clutter phenomenon. We believe that DL techniques could help to mitigate wall clutter, based on adequate simulations and appropriately designed references.

C. Potential improvements

The proposed pipeline is a relevant advance in the field of cardiac ultrasound simulation. Despite the variety of scenarios already provided, it would be of interest to integrate out-of-plane motions. Indeed, the 3-D nature of blood flow induces some decorrelation of the slow-time signals, which may affect the quality of Doppler estimates. In this study, our goal was to develop the first duplex simulation pipeline by focusing on key properties such as unsteady flow and wall clutter. The 3-D CFD model will allow us, in the future, to study and quantify the impairment caused by 3-D motion. We also evaluated the effectiveness of our simulation pipeline from healthy subjects. It would be interesting in the future to extend our framework to simulate large scale datasets including pathological cases. We will need to incorporate blood and tissue motions that reflect anatomical and functional characteristics of patients with heart disease. It should be noted however that some pathologies (e.g. valvular diseases, septal defect,...) cannot be considered due to the limitations of the CFD model.

D. Perspectives

The pipeline was used to generate an open access dataset of 20 synthetic sequences available at the following link: <http://humanheart-project.creatis.insa-lyon.fr/duplex.html>. Part of these data can already be used to benchmark the quality of Doppler estimation techniques. Our goal is to progressively enrich this dataset with new simulations to cover an exhaustive

and diverse range of blood flow dynamics, from healthy to pathological cases. This will provide richer reference datasets that will help improve the quality of flow visualization and quantification by CDI using DL methods. We are targeting three main applications in the near future. Our framework will first be used to estimate alias-free Doppler velocities from the backscattered ultrasonic signals. We have shown that our pipeline can also generate wall clutter noise. Despite a large literature dedicated to this phenomenon, clutter remains one of the main sources of error in intraventricular flow estimation. Our solution therefore offers new perspectives to develop DL-based clutter filters more efficient than the state-of-the-art (such as singular value decomposition filters). Finally, it has been shown that it was possible to decipher 2-D velocity vector fields using color Doppler images [33]. This can be used to characterize the vortex that forms in the left heart and investigate the filling capacity of the heart. The underlying method involves several tedious steps, such as segmentation of the left ventricle and aliasing/clutter filtering. We thus plan to investigate the application of DL for the automatic and robust estimation of two-dimensional intraventricular flows.

V. CONCLUSIONS

We developed a novel simulation pipeline for the generation of clinical-like duplex ultrasound sequences. The proposed pipeline combines state-of-the-art solutions in the fields of computational fluid dynamics and computational ultrasound imaging. The CFD model determines the reference value of the blood flow. The ultrasound simulator, in conjunction with scatterer strategies, ensures realistic speckle patterns and Doppler estimates. We evaluated the genericity of our pipeline in four different scenarios. In particular, we showed that our pipeline allows the integration of flow acceleration and wall clutter noise. This led to side effects and made Doppler estimation challenging, as in real cases. The pipeline was used to generate an open access dataset of 20 synthetic sequences.

This synthetic dataset can already be used to benchmark the quality of Doppler estimation techniques.

ACKNOWLEDGMENT

This work was performed within the framework of the LABEX PRIMES (ANR- 11-LABX-0063) of Université de Lyon, within the program "Investissements d'Avenir" (ANR-11-IDEX-0007) operated by the French National Research Agency (ANR).

REFERENCES

- [1] P. Pibarot, D. Garcia, and J. G. Dumesnil, "Energy loss index in aortic stenosis," *Circulation*, vol. 127, no. 10, pp. 1101–1104, 2013.
- [2] M. A. Pozniak, J. A. Zagzebski, and K. A. Scanlan, "Spectral and color doppler artifacts," *RadioGraphics*, vol. 12, no. 1, pp. 35–44, 1992.
- [3] L. Terslev, A. P. Diamantopoulos, U. M. Døhn, W. A. Schmidt, and S. Torp-Pedersen, "Settings and artefacts relevant for doppler ultrasound in large vessel vasculitis," *Arthritis Research & Therapy*, vol. 19, no. 1, p. 167, Jul 2017.
- [4] A. Shahin, M. Ménard, and M. Eboueya, "Cooperation of fuzzy segmentation operators for correction aliasing phenomenon in 3d color doppler imaging," *Artificial Intelligence in Medicine*, vol. 19, no. 2, pp. 121 – 154, 2000, medical Imaging.
- [5] S. Muth, S. Dort, I. A. Sebag, M.-J. Blais, and D. Garcia, "Unsupervised dealiasing and denoising of color-doppler data," *Medical Image Analysis*, vol. 15, no. 4, pp. 577 – 588, 2011, special section on IPMI 2009.
- [6] A. C. H. Yu and L. Lovstakken, "Eigen-based clutter filter design for ultrasound color flow imaging: a review," *IEEE Transactions on Ultrasonics, Ferroelectrics, and Frequency Control*, vol. 57, no. 5, pp. 1096–1111, 2010.
- [7] S. Fadnes, S. Bjærum, H. Torp, and L. Lovstakken, "Clutter filtering influence on blood velocity estimation using speckle tracking," *IEEE Transactions on Ultrasonics, Ferroelectrics, and Frequency Control*, vol. 62, no. 12, pp. 2079–2091, 2015.
- [8] H. Nahas, J. S. Au, T. Ishii, B. Y. S. Yiu, A. J. Y. Chee, and A. C. H. Yu, "A deep learning approach to resolve aliasing artifacts in ultrasound color flow imaging," *IEEE Transactions on Ultrasonics, Ferroelectrics, and Frequency Control*, vol. 67, no. 12, pp. 2615–2628, 2020.
- [9] O. Ronneberger, P. Fischer, and T. Brox, "U-Net: Convolutional Networks for Biomedical Image Segmentation," in *Proc. MICCAI*, 2015, pp. 234–241.
- [10] A. Madani, R. Arnaout, M. Mofrad, and R. Arnaout, "Fast and accurate view classification of echocardiograms using deep learning," *npj Digital Medicine*, vol. 1, no. 1, p. 6, Mar 2018.
- [11] S. Leclerc, E. Smistad, J. Pedrosa, A. Østvik, F. Cervenansky, F. Espinosa, T. Espeland, E. A. R. Berg, P. M. Jodoin, T. Grenier, C. Lartizien, J. D'hooge, L. Lovstakken, and O. Bernard, "Deep learning for segmentation using an open large-scale dataset in 2d echocardiography," *IEEE Transactions on Medical Imaging*, vol. 38, no. 9, pp. 2198–2210, 2019.
- [12] E. Evain, K. Faraz, T. Grenier, D. Garcia, M. De Craene, and O. Bernard, "A pilot study on convolutional neural networks for motion estimation from ultrasound images," *IEEE Transactions on Ultrasonics, Ferroelectrics, and Frequency Control*, vol. 67, no. 12, pp. 2565–2573, 2020.
- [13] A. Prakosa, M. Sermesant, H. Delingette, S. Marchesseau, E. Saloux, P. Allain, N. Villain, and N. Ayache, "Generation of synthetic but visually realistic time series of cardiac images combining a biophysical model and clinical images," *IEEE Transactions on Medical Imaging*, vol. 32, no. 1, pp. 99–109, 2013.
- [14] M. De Craene, S. Marchesseau, B. Heyde, H. Gao, M. Alessandrini, O. Bernard, G. Piella, A. R. Porras, L. Tautz, A. Hennemuth, A. Prakosa, H. Liebgott, O. Somphone, P. Allain, S. Makram Ebeid, H. Delingette, M. Sermesant, J. D'hooge, and E. Saloux, "3d strain assessment in ultrasound (strauss): A synthetic comparison of five tracking methodologies," *IEEE Transactions on Medical Imaging*, vol. 32, no. 9, pp. 1632–1646, 2013.
- [15] M. Alessandrini, M. De Craene, O. Bernard, S. Giffard-Roisin, P. Allain, I. Waechter-Stehle, J. Weese, E. Saloux, H. Delingette, M. Sermesant, and J. D'hooge, "A pipeline for the generation of realistic 3d synthetic echocardiographic sequences: Methodology and open-access database," *IEEE Transactions on Medical Imaging*, vol. 34, no. 7, pp. 1436–1451, 2015.
- [16] Y. Zhou, S. Giffard-Roisin, M. De Craene, S. Camarasu-Pop, J. D'Hooge, M. Alessandrini, D. Friboulet, M. Sermesant, and O. Bernard, "A framework for the generation of realistic synthetic cardiac ultrasound and magnetic resonance imaging sequences from the same virtual patients," *IEEE Transactions on Medical Imaging*, vol. 37, no. 3, pp. 741–754, 2018.
- [17] M. Alessandrini, B. Chakraborty, B. Heyde, O. Bernard, M. De Craene, M. Sermesant, and J. D'Hooge, "Realistic vendor-specific synthetic ultrasound data for quality assurance of 2-d speckle tracking echocardiography: Simulation pipeline and open access database," *IEEE Transactions on Ultrasonics, Ferroelectrics, and Frequency Control*, vol. 65, no. 3, pp. 411–422, 2018.
- [18] S. Marchesseau, H. Delingette, M. Sermesant, and N. Ayache, "Fast parameter calibration of a cardiac electromechanical model from medical images based on the unscented transform," *Biomechanics and Modeling in Mechanobiology*, vol. 12, no. 4, pp. 815–831, 2013.
- [19] M. Alessandrini, M. De Craene, O. Bernard, S. Giffard-Roisin, P. Allain, I. Waechter-Stehle, J. Weese, E. Saloux, H. Delingette, M. Sermesant, and J. D'hooge, "A pipeline for the generation of realistic 3d synthetic echocardiographic sequences: Methodology and open-access database," *IEEE Transactions on Medical Imaging*, vol. 34, no. 7, pp. 1436–1451, 2015.
- [20] M. Alessandrini, B. Chakraborty, B. Heyde, O. Bernard, M. De Craene, M. Sermesant, and J. D'Hooge, "Realistic vendor-specific synthetic ultrasound data for quality assurance of 2-d speckle tracking echocardiography: Simulation pipeline and open access database," *IEEE Transactions on Ultrasonics, Ferroelectrics, and Frequency Control*, vol. 65, no. 3, pp. 411–422, 2018.
- [21] C. Chnafa, S. Mendez, and F. Nicoud, "Image-based large-eddy simulation in a realistic left heart," *Computers and Fluids*, vol. 94, pp. 173–187, 2014. [Online]. Available: <https://hal.archives-ouvertes.fr/hal-00943609>
- [22] C. Chnafa, S. Mendez, R. Moreno, and F. Nicoud, *Using Image-based CFD to Investigate the Intracardiac Turbulence*. Cham: Springer International Publishing, 2015, pp. 97–117.
- [23] C. Chnafa, S. Mendez, and F. Nicoud, "Image-based simulations show important flow fluctuations in a normal left ventricle: What could be the implications?" *Annals of Biomedical Engineering*, vol. 44, no. 11, pp. 3346–3358, Nov 2016.
- [24] K. C. Assi, E. Gay, C. Chnafa, S. Mendez, F. Nicoud, J. F. P. J. Abascal, P. Lantelme, F. Tournoux, and D. Garcia, "Intraventricular vector flow mapping—a doppler-based regularized problem with automatic model selection," *Physics in Medicine & Biology*, vol. 62, no. 17, pp. 7131–7147, aug 2017.
- [25] S. Shahriari and D. Garcia, "Meshfree simulations of ultrasound vector flow imaging using smoothed particle hydrodynamics," *Physics in Medicine & Biology*, vol. 63, no. 20, p. 205011, 2018.
- [26] D. Garcia, "Simus: an open-source simulator for ultrasound imaging. part i: theory & examples," 2021.
- [27] V. Perrot, M. Polichetti, F. Varray, and D. Garcia, "So you think you can das? a viewpoint on delay-and-sum beamforming," *Ultrasonics*, vol. 111, p. 106309, 2021.
- [28] C. Madiena, J. Faurie, J. Porée, and D. Garcia, "Color and vector flow imaging in parallel ultrasound with sub-nyquist sampling," *IEEE Transactions on Ultrasonics, Ferroelectrics, and Frequency Control*, vol. 65, no. 5, pp. 795–802, 2018.
- [29] J. Faurie, M. Baudet, K. C. Assi, D. Auger, G. Gilbert, F. Tournoux, and D. Garcia, "Intracardiac vortex dynamics by high-frame-rate doppler vortography—*in vivo* comparison with vector flow mapping and 4-d flow mri," *IEEE Transactions on Ultrasonics, Ferroelectrics, and Frequency Control*, vol. 64, no. 2, pp. 424–432, 2017.
- [30] J. Faurie, M. Baudet, J. Porée, G. Cloutier, F. Tournoux, and D. Garcia, "Coupling myocardium and vortex dynamics in diverging-wave echocardiography," *IEEE Transactions on Ultrasonics, Ferroelectrics, and Frequency Control*, vol. 66, no. 3, pp. 425–432, 2019.
- [31] A. Østvik, I. M. Salte, E. Smistad, T. M. Nguyen, D. Melichova, H. Brunvand, K. Haugaa, T. Edvardsen, B. Grenne, and L. Lovstakken, "Myocardial function imaging in echocardiography using deep learning," *IEEE Transactions on Medical Imaging*, vol. 40, no. 5, pp. 1340–1351, 2021.
- [32] A. Nilsson, "Artefacts in sonography and doppler," *European Radiology*, vol. 11, no. 8, pp. 1308–1315, Aug. 2001.
- [33] D. Garcia, J. C. del Alamo, D. Tanné, R. Yotti, C. Cortina, E. Bertrand, J. C. Antoranz, E. Pérez-David, R. Rieu, F. Fernandez-Avilés, and J. Bermejo, "Two-dimensional intraventricular flow mapping by digital processing conventional color-doppler echocardiography images," *IEEE Transactions on Medical Imaging*, vol. 29, no. 10, pp. 1701–1713, 2010.